Research Article

Mohammad Abdollahi-Alibeik* and Zahra Ramazani

Core–shell structured magnetic MCM-41-type mesoporous silica-supported Cu/Fe: A novel recyclable nanocatalyst for Ullmann-type homocoupling reactions

https://doi.org/10.1515/mgmc-2022-0018
received January 05, 2022; accepted June 28, 2022

Abstract: In this study, a novel magnetic MCM-41-type mesoporous silica-supported Fe/Cu (Fe_3O_4@Fe–Cu/MCM-41) was prepared, characterized, and used as a heterogeneous catalyst for the synthesis of symmetric biaryls by Ullmann cross-coupling reaction. This nanocomposite was characterized using Fourier transform infrared spectroscopy, energy-dispersive X-ray spectroscopy, X-ray diffraction, and nitrogen adsorption–desorption isotherm. The Fe_3O_4@Fe–Cu/MCM-41 was applied as an efficient catalyst in the synthesis of biaryls under optimum conditions. This nanocatalyst was recovered and reused several times without significant loss of activity.

Keywords: MCM-41, Fe_3O_4, mesoporous silica, nanocatalyst, Ullmann homocoupling, biaryls

1 Introduction

Since the discovery of the Ullmann reaction in 1901 (Niemelä, 1987), it has been known as one of the most important synthetic pathways to biaryls using carbon–carbon coupling reaction (Chen et al., 2020; Dai et al., 2019). The coupling of aryl halides with different compounds containing O, N, S, P, and C elements by the Ullmann reaction cause the formation of P–, S–, O–, N–, and C–aryl bonds (Galeotti et al., 2019; Hemmati et al., 2020; Hosseinian et al., 2019; Khalili et al., 2019). Among the products of various coupling, symmetric biaryls obtained from the C–C bonds coupling of aryl halides are very important as active precursors for the synthesis of many pharmaceutically active compounds, herbicides, polymers, new materials, liquid crystals, and ligands (Khodaei et al., 2019; Kitanovski, 2020).

The Ullmann reaction generally proceeds in the presence of different heterogeneous and homogeneous catalysts containing various metals such as Au (Rodríguez-Fernández et al., 2018) Cu (Yavari et al., 2019), Pd/Ni (Sakata et al., 2018), Pd^0 (Seyedi et al., 2019; Wang et al., 2020), and cellulose nanocrystal-supported palladium (Seyednejhad et al., 2019) as catalysts. However, the use of homogeneous catalysts suffers from several limitations such as recovery and separation from the reaction media (Abaeezadeh et al., 2019; Esrafili et al., 2020). So, it is very important to find a suitable alternative to homogeneous catalysts (Cha et al., 2020; Chatterjee et al., 2019; Elhamifar et al., 2018). In recent decades, heterogeneous catalysts have become an alternative to homogeneous catalysts to overcome problems such as reusability and easy separation from the reaction media which is a significant and important challenge of chemistry processes (Abdollahi-Alibeik et al., 2020; Javid and Moeinpour, 2018; Khalilzadeh et al., 2020; Zarei et al., 2020).

Nanomaterials have received considerable attention in chemistry and material areas due to their unique physical and chemical properties and also their applications in various fields such as waste removal, degradation of different pollutants such as dyes and toxic metals, catalyst and catalyst support (Bahrami et al., 2020; Eivazzadeh-Keihan et al., 2021; Liu et al., 2019; Maleki, 2018; Maleki et al., 2019, 2020; Nasrallah et al., 2018). Among the various types of nanomaterials, magnetic iron oxide nanoparticles (MNPs) have received a lot of attention because of their high surface area, non-toxicity, easy availability, easy separation, and recovery using an external

* **Corresponding author: Mohammad Abdollahi-Alibeik,** Department of Chemistry, Yazd University, Yazd 89158-13149, Iran, e-mail: abdollahi@yazd.ac.ir, tel: +98-35-31232659, fax: +98-35-38210644
Zahra Ramazani: Department of Chemistry, Yazd University, Yazd 89158-13149, Iran, e-mail: moabdollahi@gmail.com

Open Access. © 2022 Mohammad Abdollahi-Alibeik and Zahra Ramazani, published by De Gruyter. This work is licensed under the Creative Commons Attribution 4.0 International License.

magnet (Nikoorazm and Erfani, 2019; Norouzi et al., 2018; Ojaghi Aghbash et al., 2019). Due to their unique properties, magnetic NPs have been used in various applications such as drug delivery and catalysts in chemical processes (Daneshafruz et al., 2022; Hashemi-Uderji et al., 2018a; Pourhasan-Kisomi et al., 2019; Ramazani et al., 2019; Reiss et al., 2009).

However, magnetic nanoparticles are very unstable in acidic and basic media. To solve this problem, various species such as silica, metal oxides, polymers, surfactants, and carbon have been used as a shell for the stabilization of magnetic cores (Abdollahi-Alibeik and Rezaeipoor-Anari, 2016; Sobhan Ardakani et al., 2020). Among the mentioned coating, silica coating is the best because silica-coated nanoparticles can be easily modified by their silanol group (Adlnasab et al., 2018; Moaddeli and Abdollahi-Alibeik, 2017).

Among the various types of silica coatings, mesoporous silica is very noticeable and widely applied as a catalyst in chemical processes due to its notable features such as tunable physical and chemical properties, easy preparation, high surface area, low cost, high flexibility, and high availability (Abdollahi-Alibeik and Moaddeli, 2015; Hajian and Ehsanikhah, 2018; Hashemi-Uderji et al., 2018c). So, recently magnetic mesoporous silica materials have been considered active catalyst support because of having advantages of both MNPs and mesoporous silica such as simple recoverability and easy separation (Hashemi-Uderji et al., 2018b; Nikoorazm et al., 2018; Xie et al., 2018). Several magnetic nanostructured silica catalysts are prepared and applied in chemical processes such as $Fe_3O_4@SiO_2$ (Maleki, 2012, 2013), $Fe_3O_4@SiO_2–OSO_3H$ (Maleki, 2014), $Fe_3O_4/SiO_2/o$-PDA (Maleki et al., 2020), Cu_2O/agar@Fe_3O_4 (Maleki et al., 2019), $Fe_3O_4@SiO_2–NH_2$ (Maleki and Azadegan, 2017), Fe_3O_4@MCM-41@Pd-SPATB (Nikoorazm et al., 2018), Rd-MCM-41@Fe_3O_4 (Chen and Mu, 2014), $Yb(OTf)_2$-SO_3Na&Ph-MCMSS (Zhang et al., 2014), Fe_3O_4@MCM-41-SH (Ulu et al., 2018), Fe_3O_4@MCM-41-Im@MnPor (Hajian and Ehsanikhah, 2018), and Mag@MCM-41/TiO_2 (Vahidian et al., 2020).

In this article, the synthesis and characterization of a novel magnetic mesoporous silica containing iron and copper oxides (Fe_3O_4@Fe–Cu/MCM-41) with core–shell structure is developed. Moreover, the catalytic application of Fe_3O_4@Fe–Cu/MCM-41 is studied in the Ullmann-type homocoupling reaction to produce biaryls (Scheme 1).

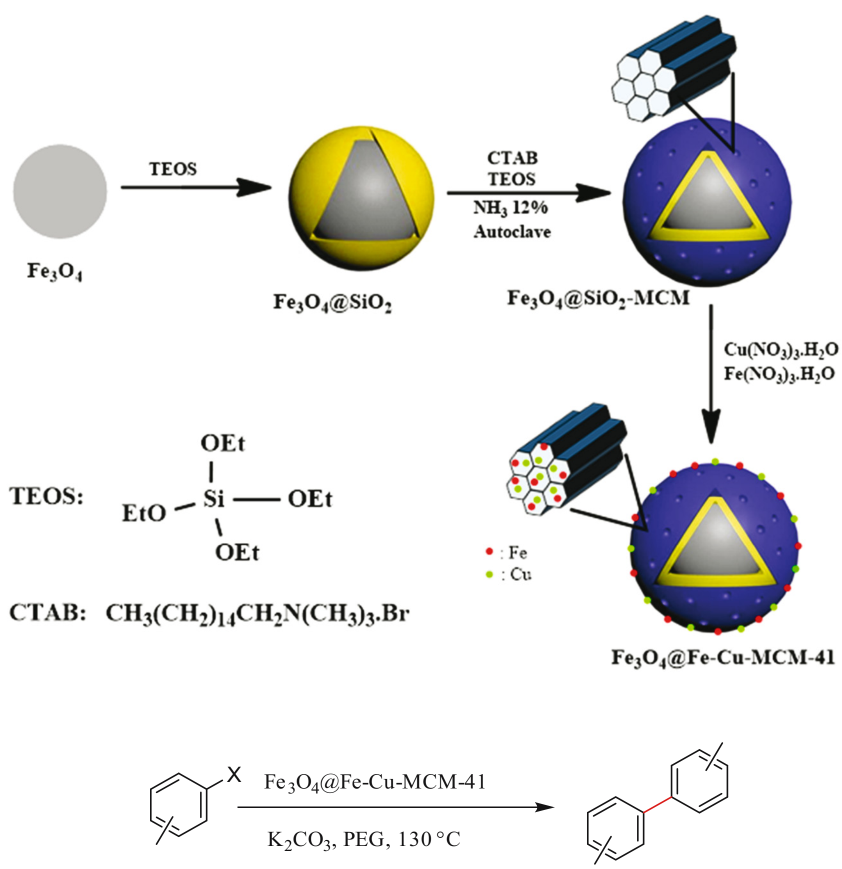

Scheme 1: Preparation of Fe_3O_4@Fe–Cu/MCM-41 nanocomposite and its application in the Ullmann reaction.

2 Results and discussion

In this research, a novel core–shell catalyst containing Fe and Cu with Fe_3O_4 core and MCM-41 shell was prepared and characterized, and its catalytic application was studied in the synthesis of biaryls. The synthesis procedure for Fe_3O_4@Fe–Cu/MCM-41 nanocomposite is shown in Scheme 1. The Fe_3O_4@Fe–Cu/MCM-41 samples with molar ratios of Si:Fe/Si:Cu (mole of Si in the MCM-41) = 20:1/20:1, 30:1/30:1, 40:1/40:1, 60:1/40:1, and 40:1/60:1 were prepared and denoted as FCMS(20:20), FCMS(30:30), FCMS (40:40), FCMS(60:40), and FCMS(40:60), respectively.

The chemical and physical properties of the synthesized catalyst were investigated using Fourier transform infrared (FT-IR) spectroscopy, Nitrogen adsorption–desorption isotherm, low-angle X-ray diffraction (XRD), transmission electron microscopy (EDX), and mappings analysis.

The FT-IR analysis of Fe_3O_4, Fe_3O_4@SiO_2, Fe_3O_4@MCM-41, and Fe_3O_4@Fe–Cu/MCM-41 (FCMS(20:20)) was performed to study the functionality of the nanoparticles (Figure 1). For all samples, the characteristic peak of the Fe–O bond is observed at about 622 cm^{-1} and the sharp peaks cleared at 1,637 cm^{-1} are assigned to OH bending vibrations of the material surface. In the spectra of the Fe_3O_4@SiO_2 (Figure 1b), Fe_3O_4@MCM-41 (Figure 1c), Fe_3O_4@Fe–Cu/MCM-41 (Figure 1d), the sharp bands appeared at 1,084 and 804 cm^{-1} are attributed to asymmetric and symmetric stretching vibrations of Si–O–Si bonds. In the spectrum of Fe_3O_4@MCM-41, the band at 961 cm^{-1} is attributed to the Si–OH group (Figure 1c), which is lost in the spectrum of Fe_3O_4@Fe–Cu/MCM-41 due to the bonding of Fe and Cu with the surface of the MCM-41 (Figure 1d).

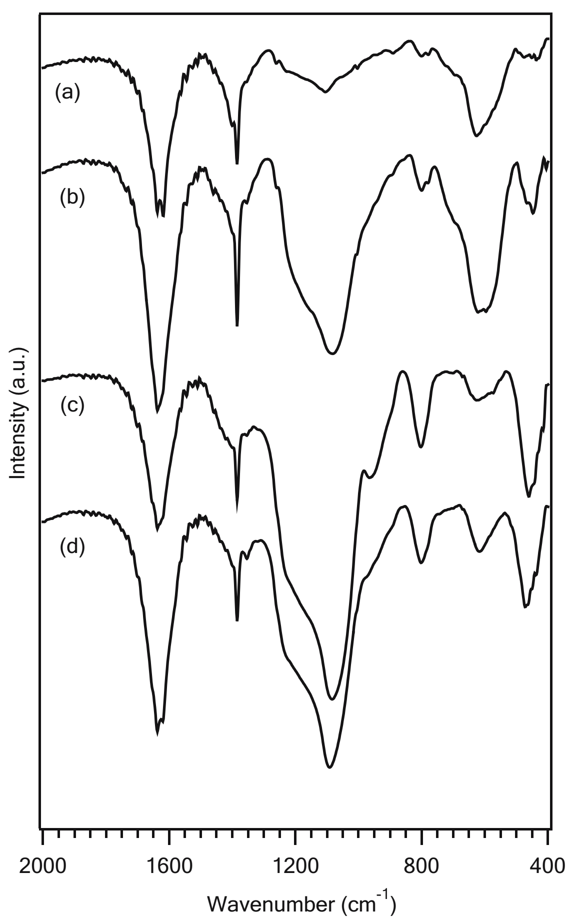

Figure 1: FT-IR spectra of (a) Fe_3O_4, (b) Fe_3O_4@SiO_2, (c) Fe_3O_4@MCM-41, and (d) Fe_3O_4@Fe–Cu/MCM-41.

High-angle XRD patterns of Fe_3O_4, Fe_3O_4@MCM-41, and Fe_3O_4@Fe–Cu/MCM-41 nanocomposite are shown in Figure 2. Fe_3O_4 shows diffraction peaks at 2θ = 26.2, 35.6, 44.2, 53.6, 58.1, and 62.9° that are indexed to the crystalline cubic inverse spinel structure of Fe_3O_4 nanoparticles (Figure 2a) (Wang et al., 2010). In the XRD pattern of Fe_3O_4@MCM-41, in addition to the main peaks of Fe_3O_4, a broad peak at 2θ = 24° corresponding to the amorphous structure of silica walls of MCM-41 is observed (Figure 2b). In the XRD pattern of Fe_3O_4@Fe–Cu/MCM-41 nanocomposite, except for the peak at 2θ = 26.2° which overlaps with the broad peak of the amorphous structure of silica, all Fe_3O_4 peaks are observed. This shows the high stability of the crystalline structure of Fe_3O_4 NPs during catalyst preparation. Also, the metals phase does not appear in the high-angle XRD pattern, which shows high dispersion of copper and ferric ions in the MCM-41 framework.

The representative low-angle X-ray diffraction (LAXRD) pattern of Fe_3O_4@Fe–Cu/MCM-41 nanocomposite is offered in Figure 3. This pattern shows a peak with high intensity at 2θ = 2.2° which is attributed to the two-dimension hexagonal mesostructure of the supported MCM-41 shell (Figure 3). The decrease in 2θ based on Bragg's equation and also broadening are observed at low-angle XRD pattern of Fe_3O_4@Fe–Cu/MCM-41 compared to pure MCM-41, which is due to the decrease in the ordered degree of hexagonal mesostructures after connection of magnetic iron oxide into the MCM-41 framework. These changes are also due to the bonding of Fe and Cu to the surface of the MCM-41.

The energy-dispersive X-ray sepectroscopy (EDS) was studied to apperceive the type of elements in the Fe_3O_4@Fe–Cu/MCM-41 nanocomposite. The template indicated the presence of Si, O, Cu, and Fe in the material proving successful incorporation (Figure 4).

The EDX mapping analysis was also executed to investigate the immobilization and dispensation of Fe, Cu, Si, and O elements in the material network (Figure 5a–d).

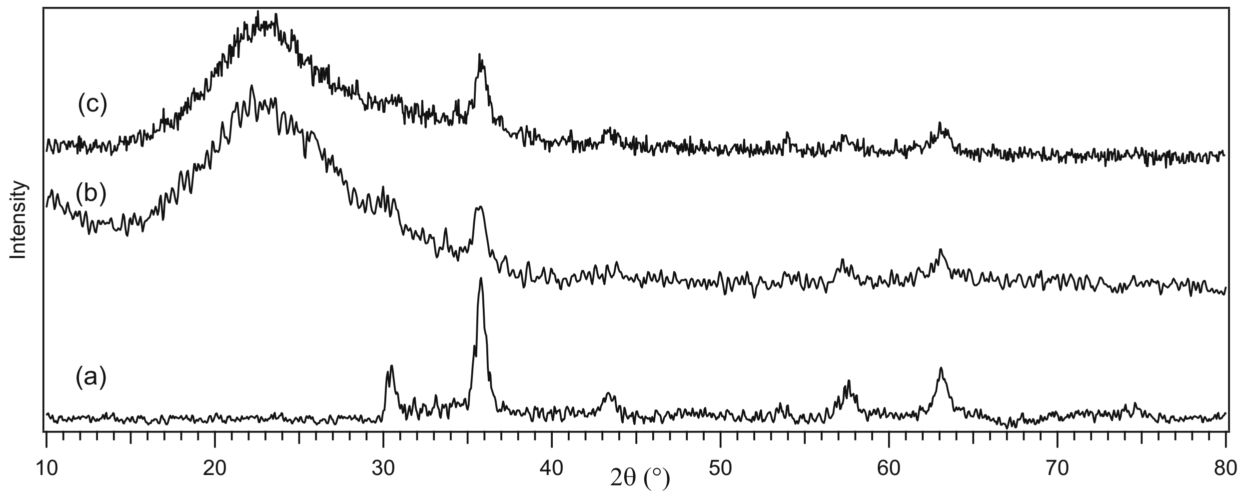

Figure 2: High-angle XRD analysis of the (a) Fe_3O_4, (b) Fe_3O_4@MCM-41, and (c) Fe_3O_4@Fe–Cu/MCM-41 nanocomposite.

As shown in Figure 5a, the Fe element shows a cumulative state because it exists in the catalyst structure in two forms Fe_3O_4 and Fe. But Cu element is distributed almost uniformly on the surface of the catalyst (Figure 5b) which this pattern corresponds to the XRD analysis, where no crystalline phase of copper was observed. However, these results and also XRD analysis show that both of these elements are distributed almost uniformly on the surface of the catalyst.

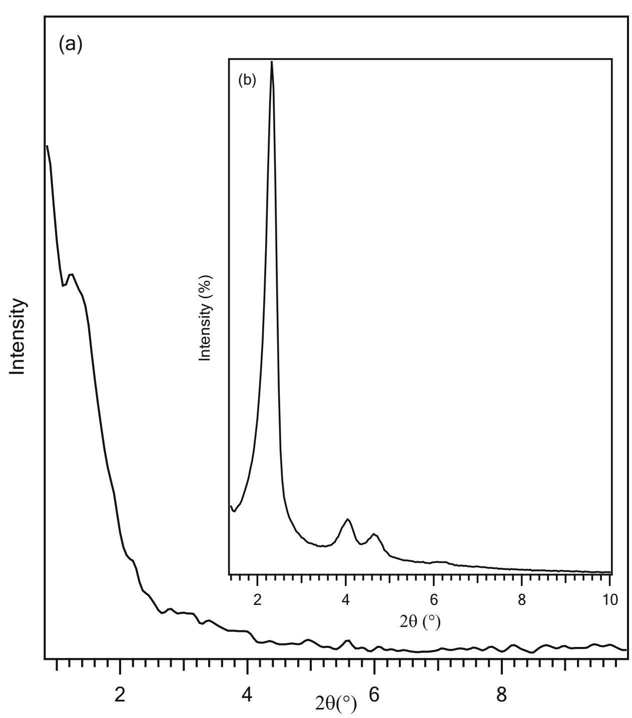

Figure 3: Low-angle XRD analysis of (a) Fe_3O_4@Fe–Cu/MCM-41 and (b) MCM-41.

In order to investigate the preservation of the mesoporous structure of the catalyst after being placed around the Fe_3O_4 core as well as the arrival of the Cu and Fe elements on the surface, the nitrogen adsorption–desorption isotherms for the Fe_3O_4@Fe–Cu/MCM-41 catalyst are depicted in Figure 6. This isotherm exposes the existence of well-defined mesopores. In this isotherm, a sharp inflection at $p/p° = 0.3–0.4$ is related to the nitrogen capillary condensation in the uniform mesopores, which confirms the mesoporous structure of synthesized Fe_3O_4@Fe–Cu/MCM-41. The textural properties of Fe_3O_4@Fe–Cu/MCM-41 were also studied by N_2 adsorption–desorption isotherms. The results show that the Brunauer-Emmett-Teller (BET) surface area and pore volume of the MCM-41 substantially decrease from 1,050 to 514 $m^2·g^{-1}$ and 1.647 to 1.050 $cm^3·g^{-1}$, respectively, due to the entrance of Fe_3O_4 in MCM-41 framework and

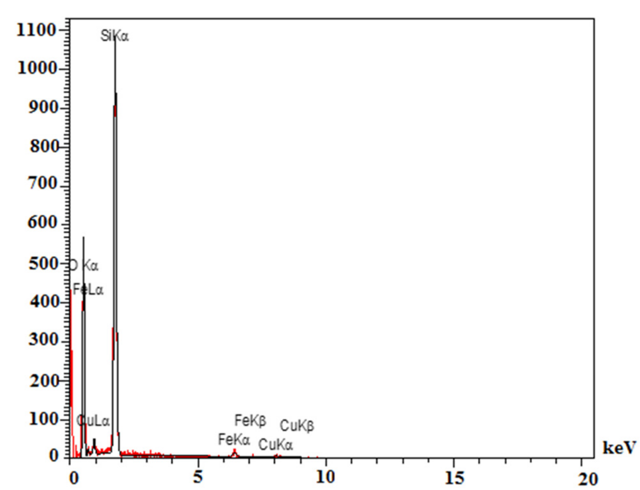

Figure 4: EDX analysis of Fe_3O_4@Fe–Cu/MCM-41 nanocatalyst.

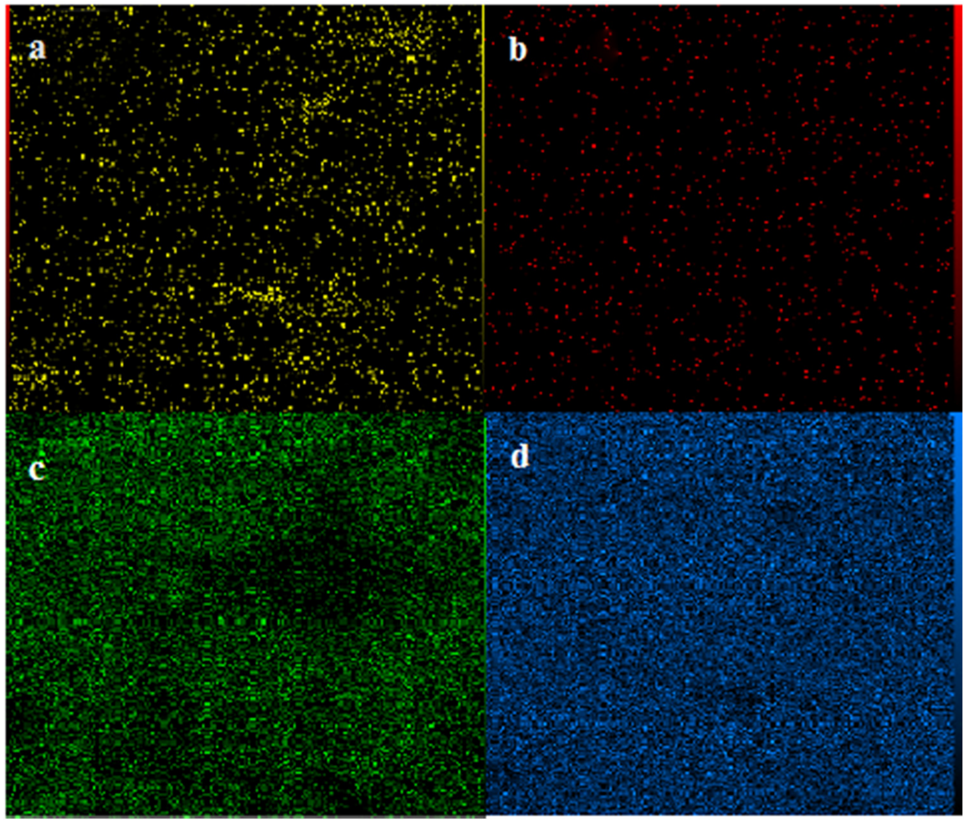

Figure 5: EDX mapping of the Fe_3O_4@Fe–Cu/MCM-41 nanocatalyst. (a) Fe, (b) Cu, (c) O, and (d) Si.

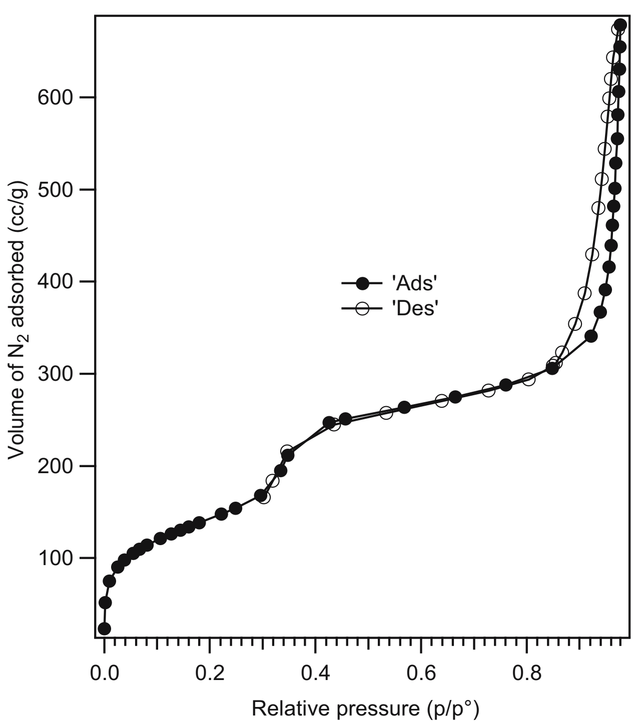

Figure 6: Nitrogen adsorption–desorption isotherm of the Fe_3O_4@Fe–Cu/MCM-41 nanocatalyst.

also impregnation of Fe and Cu on the inner surface of mesoporous channels of MCM-41.

To study the magnetic property of Fe_3O_4@Fe–Cu/MCM-41, magnetic measurements were performed using a room

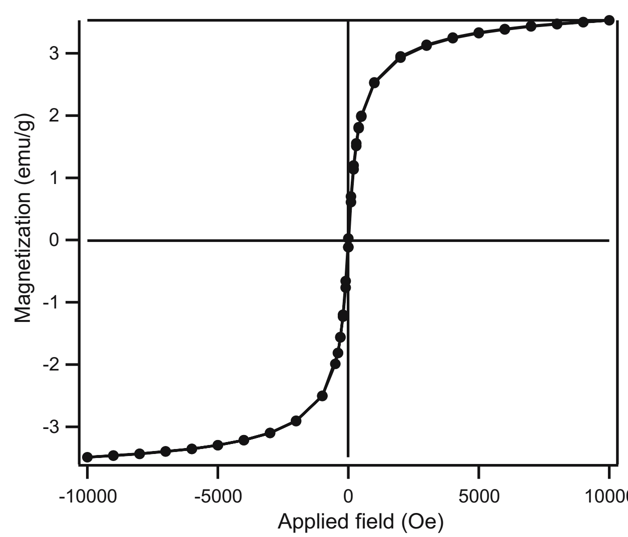

Figure 7: Magnetization versus applied magnetic field curve of Fe_3O_4@Fe–Cu/MCM-41.

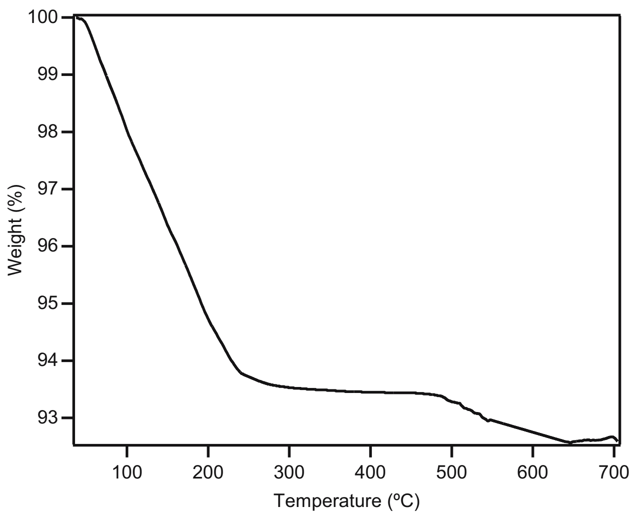

Figure 8: TGA analysis of sample under flowing air at a heating rate of 10°C·min^{-1}.

temperature vibrating sample magnetometer (VSM) in an applied magnetic field. As shown in Figure 7, the typical superparamagnetic nature at 300k is corroborated by not observing any hysteresis loops and also zero coercivity value.

The thermal properties of the samples were investigated using thermogravimetric analysis (TGA), and the result is shown in Figure 8. TGA of the sample showed two steps of weight loss. The first weight loss step is located from room temperature to 275°C due to the desorption of physically adsorbed water and hydrogen-bonded water on the MCM-41. The second weight loss step from 485°C to 650°C is due to residual silanol condensation of adjacent Si–OH groups to form siloxane bonds.

After the characterization of Fe_3O_4@Fe–Cu/MCM-41, its role as a heterogeneous nanocatalyst was evaluated in the Ullmann-type homocoupling reactions for C–C bond formations (Scheme 1). For this purpose, the reaction of 4-nitrobromobenzen was chosen as the model reaction, and the effect of some important parameters such as solvent, temperature and catalyst loading was studied to obtain the best reaction conditions (Table 1). As shown in Table 1, to study the effect of the catalyst loading on the progress of the reaction, the model reaction was carried

Table 1: The effect of solvent, temperature, and catalyst loading in the Ullmann-type homocoupling reaction

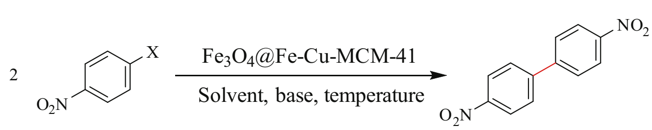

Entry	Catalyst	Catalyst amount (mg)	Solvent	Base	Temperature (°C)	Time (h:min)	Yield* (%)
1	—	—	PEG-200	K_2CO_3	140	24:00	0
2	FCMS(60:60)	80	PEG-200	K_2CO_3	130	4:30	83
3	FCMS(40:40)	80	PEG-200	K_2CO_3	130	3:40	80
4	FCMS(30:30)	80	PEG-200	K_2CO_3	130	2:15	86
5	FCMS(40:60)	80	PEG-200	K_2CO_3	130	4:00	90
6	FCMS(60:40)	80	PEG-200	K_2CO_3	130	4:05	93
7	FCMS(20:20)	50	PEG-200	K_2CO_3	130	3:20	80
8	FCMS(20:20)	70	PEG-200	K_2CO_3	130	2:00	94
9	FCMS(20:20)	100	PEG-200	K_2CO_3	130	1:20	86
10	FCMS(20:20)	80	PEG-200	K_2CO_3	130	1:20	94
11	FCMS(20:20)	80	PEG-200	K_2CO_3	140	1:20	93
12	FCMS(20:20)	80	PEG-200	K_2CO_3	100	2:00	90
13	FCMS(20:20)	80	PEG-200	K_2CO_3	80	2:30	90
14	FCMS(20:20)	80	PEG-200	K_2CO_3	65	6:00	86
15	FCMS(20:20)	80	PEG-200	K_2CO_3	50	7:30	80
16	FCMS(20:20)	80	PEG-200	K_2CO_3	R.T	10:00	60
17	FCMS(20:20)	80	—	K_2CO_3	130	10:00	0
18	FCMS(20:20)	80	H_2O	K_2CO_3	130	3:00	50
19	FCMS(20:20)	80	EtOH	K_2CO_3	130	4:45	30
20	FCMS(20:20)	80	DMSO	K_2CO_3	130	7:00	30
21	FCMS(20:20)	80	PEG-200	Na_2CO_3	130	1:30	90
22	FCMS(20:20)	80	PEG-200	KOH	130	2:40	85
23	FCMS(20:20)	80	PEG-200	Cs_2CO_3	130	4:00	45
24	FCMS(20:20)	80	PEG-200	Na_3PO_4	130	3:40	40

*Isolated yield.

Table 2: Preparation of biaryl derivatives in the presence of Fe3O4@Fe–Cu/MCM-41*

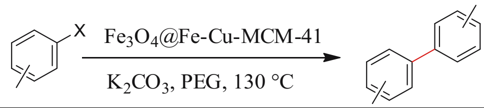

Entry	Aryl halide	Product	Time (min)	Yield** (%)	TON	TOF (h^{-1})
1	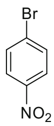	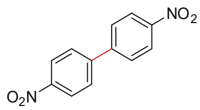	80	94	9.4	7
2	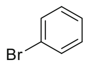	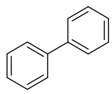	155	89	8.9	3.4
3	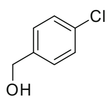	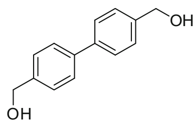	300	90	9	1.8
4	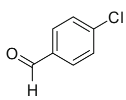	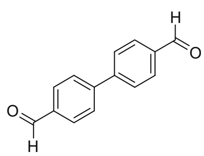	210	86	8.6	2.4
5	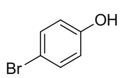	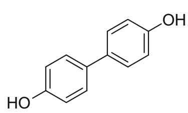	140	90	9	3.8
6	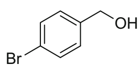	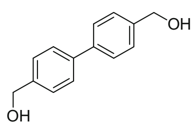	140	90	9	3.8
7	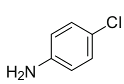	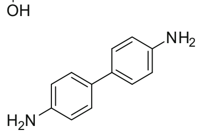	250	90	9	2.1
8	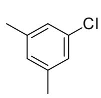	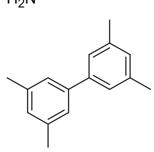	120	92	9.2	4.6
9	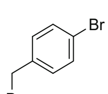	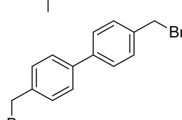	240	85	8.5	2.1
10	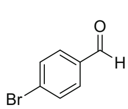	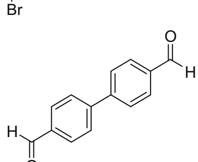	180	89	89	2.2
11	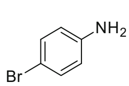	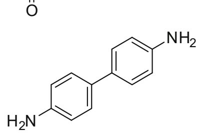	240	90	9	2.2
12	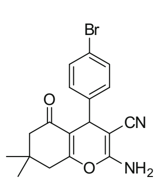	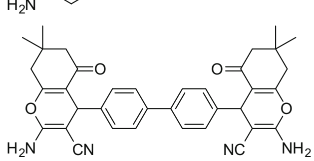	160	91	9.1	3.4

*Reaction conditions: aryl halides (2 mmol), K_2CO_3 (1 equiv.), PEG (2.5 mL), Fe_3O_4@Fe–Cu/MCM-41 (80 mg), and $T = 130$°C.
** Isolated yields.

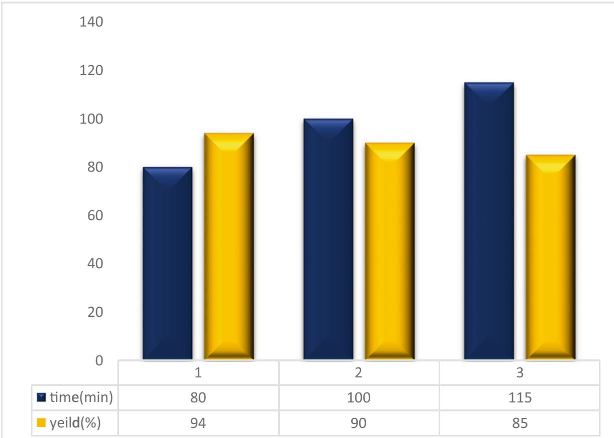

Figure 9: Reusability of the Fe_3O_4@Fe–Cu/MCM-41 nanocatalyst in the Ullmann reaction.

out in the absence of the catalyst under reflux for 24 h, and in this condition, no product was obtained (Table 1, entry 1). Next, the reaction in the presence of the prepared catalyst samples with different amounts of the molar ratios of SiO_2:Fe:Cu was checked, and the best result was obtained using the molar ratio of Si:Fe:Cu = 20:1:1 (FCMS(20:20)) (Table 1, entries 2–7). To investigate the effect of the catalyst amount, the model reaction was performed in the presence of different amounts of the catalyst from 50 to 100 mg (Table 1, entries 7–10). The results show that with increasing the catalyst amounts to 80 mg, a substantial improvement was observed in both reaction time and product yield. The temperature also affected the reaction progress, and excellent conversion was obtained at 130°C (Table 1, entry 10). Also, to investigate the effect of solvent on the reaction time and product yield, the model reaction was performed in common solvents such as PEG-200, EtOH, DMSO, water, and also in solvent-free conditions (Table 1, entries 18–20). The effect of the use of various bases such as Na_2CO_3, KOH, Na_3PO_4, Cs_2CO_3, and K_2CO_3 was studied, and the results are shown in Table 1 (entries 21–24). The results showed that the best condition for the coupling reaction of aryl halide (2 mmol) is the use of 80 mg (0.5 mol% of Fe and Cu) FCMS(20:20) nanocatalyst and K_2CO_3 (2 mmol) as the base in the presence of PEG-200 (2.5 mL) as a solvent at 130°C (Table 1, entry 10).

To investigate the role of mesoporous channels of MCM-41 as catalyst support for metals in the Ullman reaction, the Fe_3O_4@SiO_2 was used as catalyst support and Fe_3O_4@Fe–Cu/SiO_2 was prepared with the same amounts of Cu and Fe in the main catalyst. The latter catalyst was compared with Fe_3O_4@Fe–Cu/MCM-41 in the model reaction under the same condition. The reaction time increased from 80 min. when using Fe_3O_4@Fe–Cu/MCM-41 to 390 min. and Fe_3O_4@Fe–Cu/SiO_2, and a decrease in the yield from 94% to 65%, respectively, show the role of mesoporous channels of MCM-41 in increasing the surface of the catalyst as well as the role of MCM-41 channels as nanoreactors to bring the reactants closer together.

After identifying the optimized reaction conditions, the substrate scope of this catalytic system was studied (Table 2). As shown, aryl halides with electron-donating functional groups as well as electron-withdrawing bearing aryl halides were applied as substrate and delivered corresponding biaryls in high to excellent yield (Table 2). It was found that the substituent group on the benzene ring has a certain influence on the reaction. A higher yield and shorter reaction time were obtained when the substituent group is a highly electron-withdrawing group such as a nitro group (Table 2, entry 1). When a substituent group is an electron-donating group such as amine, only a moderate yield in a longer reaction time can be obtained. However, in the presence of heterogeneous catalysts, where the adsorption of the substrate on the surface is important, another factor involved in the reactivity of the substrate is the interaction of different positions of the substrate on the surface of the catalyst, which may not be related to the electron-withdrawing or electron-donating properties of the functional groups.

One of the important advantages of heterogeneous catalysts could be their recyclability and reusability. In the next stage, the recovery and the reusability of the Fe_3O_4@Fe–Cu/MCM-41 nanocatalyst were studied on the model reaction under the optimized conditions for the Ullmann homocoupling reaction (Figure 9). For this, after

Table 3: Comparison of catalytic activity of Fe_3O_4@Fe–Cu/MCM-41 nanocatalyst with several known catalysts

Entry	Catalyst	Catalyst loading	Condition	Time	Yield (%)	Ref
1	PS-PdNPS	1.5 mol%	H_2O, additive, 80°C, NaOH	3 h	85	(Ohtaka et al., 2018)
2	MOF-235.0.05PdCl_2	1 mol%	DMSO:EtOH, 120°C, KOAc	10 h	>99	(Chen et al., 2015)
3	m@ZIF-8	6 mmol%	DMF, 140°C, K_3PO_4	48 h	100	(Wang et al., 2020)
4	Au-Pd@NMCl-2	1 mol%	H_2O/EtOH, R.T, K_2CO_3	6 h	95	(Karimi et al., 2018)
5	Fe_3O_4@Fe–Cu/MCM-41	0.5 mmol%	PEG, 130°C, K_2CO_3	1 h:20 min	94	In this work

completion of the reaction, the catalyst was easily separated from the reaction mixture by an external magnetic field and washed with hot ethanol. Then, it was reused in the next run under the same conditions as the first run. The study showed that the catalyst could be recovered and reused at least three times without a significant reduction in efficiency (Figure 9).

To demonstrate the efficiency and capability of the Fe_3O_4@Fe–Cu/MCM-41 nanocatalyst for the Ullmann reaction, it has been compared with those reported in the literature mediated by other catalysts (Table 3). As is evident from Table 3, the Fe_3O_4@Fe–Cu/MCM-41 nanocatalyst is superior to some of those previously reported in the reaction conditions, reaction time, and recycling times. The high efficiency of the nanocatalyst is attributed to stability, high uniformity, highly mesoporous structure of the material, and high surface area of the design catalyst.

3 Conclusion

In conclusion, in this study, we have reported the preparation, characterization, and catalytic application of a novel Fe/Cu-containing core–shell material with Fe_3O_4 core, SiO_2, and nanoporous MCM-41 shell (Fe_3O_4@Fe–Cu/MCM-41). The FT-IR and EDX analyses successfully confirmed well immobilization and high stability of magnetic iron oxide cores. The low-angle XRD pattern showed the presence of a well-ordered mesoporous silica shell around magnetic particles. The wide-angle XRD analysis demonstrated high stability of the crystalline structure of MNPs during the synthesis process. The Fe_3O_4@Fe–Cu/MCM-41 (80 mg) was effectively and powerfully applied in the synthesis of biaryls at 130°C in PEG-200 (2.5 mL) as a solvent and delivered desired products in high to excellent yield. The best molar ratio of Si:Fe:Cu for the preparation of the catalyst is 20:1:1. Reusability study shows that nanocatalysts could be recovered and reused several times without noticeable loss of catalytic activity. Simple workup, high product yields, and easy recovery of the catalyst are some advantages of this catalyst.

Experimental section

Preparation of Fe_3O_4@SiO_2 nanoparticles

The magnetic Fe_3O_4 nanoparticles were prepared via an improved chemical precipitation method (Abdollahi-Alibeik and Rezaeipoor-Anari, 2016). According to this method, $FeCl_2·4H_2O$ (1.52 g, 8 mmol) and $FeCl_3·6H_2O$ (4.2 g, 16 mmol) were dissolved in deionized water (100 mL), and then, the temperature was increased to 50–60°C under nitrogen atmosphere. Then, ammonia solution (30 mL, 25 wt%) was slowly added to the solution and mixed for 60 min at 60°C. The obtained magnetic nanoparticles were separated using an external magnet and washed several times with deionized water and then was dried at 80°C for 6 h. The surface of Fe_3O_4 NPs was covered by a SiO_2 shell through Stöber method (Stöber et al., 1968). Fe_3O_4 nanoparticles (1 g), ammonia (4 mL, 25 wt%), deionized water (20 mL), and ethanol (70 mL) were mixed under ultrasonic conditions at room temperature for 10 min. Then, TEOS (0.5 mL) was added to the mixture and stirred for 8 h at room temperature. The obtained magnetic nanoparticles (Fe_3O_4@SiO_2) were separated using an external magnet and washed several times with water and absolute ethanol (3 mL × 3 mL). The product was dried in a vacuum oven at 80°C for 6 h.

Preparation of Fe_3O_4@MCM-41 nanoparticles

Fe_3O_4@SiO_2 nanoparticles (0.066 g, 0.284 mmol) were dispersed in distilled water (100 mL) by ultrasonic waves for 10 min at room temperature. After complete dispersion of Fe_3O_4@SiO_2 nanoparticles, cetyltrimethylammonium bromide (CTAB) (0.52 g, 1.45 mmol) was slowly added to the mixture and stirred at 70°C for 1 h. Then, TEOS (2.5 mL, 12 mmol) was added to the reaction vessel and stirred for 1 h. After that, an ammonia solution of 12% were added drop-wise to the reaction mixture to reach pH = 10.2. Lastly, the mixture was transferred to an autoclave and hydrothermally treated in an oven at 120°C for 12 h under static. After completion of the reaction, the resulting product was separated by an external magnet and washed with EtOH and water (2 mL × 3 mL), dried at 120°C for 2 h, and then further heated in an air oven at 450°C for 6 h.

Preparation of Fe_3O_4@Fe–Cu/MCM-41 nanoparticles

A mixture of Fe_3O_4@MCM-41, $Fe(NO_3)_3·9H_2O$ (29 mg, 0.072 mmol), and $Cu(NO_3)_3·3H_2O$ (17 mg, 0.072 mmol) in deionized water (2.5 mL) was mechanically stirred at room temperature for 1 h. Subsequently, the temperature was increased slowly and the solvent gradually came out. Then, the resulting product was dried in a vacuum oven at 120°C for 2 h and then further heated in an air oven at 450°C for 6 h.

Procedure for the synthesis of biaryls using Fe_3O_4@Fe–Cu/MCM-41 catalyst

A mixture of Fe_3O_4@Fe–Cu/MCM-41 (FCMS(20:20)) (80 mg), aryl halide (2 mmol), K_2CO_3 (2 mmol), and PEG-200 (2.5 mL) was heated at 130°C. The reaction progress was monitored using TLC (eluent: EtOAc:*n*-hexane; 80:20). After completion of the reaction, hot ethanol (4 mL) was added, and the catalyst was removed via a magnetic field. Finally, the crude product was taken in ethyl acetate, and the organic layer was washed using brine solution and dried over magnesium sulfate. The solvent was evaporated to obtain the pure product in 94% yield.

Funding information: The authors state no funding involved.

Author contributions: Mohammad Abdollahi-Alibeik: supervision, writing – review and editing, methodology, project administration; Zahra Ramazani: writing – original draft, experimental analysis; resources.

Conflict of interest: The authors state no conflict of interest.

References

Abaeezadeh S., Elhamifar D., Norouzi M., Shaker M., Magnetic nanoporous MCM-41 supported ionic liquid/palladium complex: An efficient nanocatalyst with high recoverability. Appl. Organomet. Chem., 2019, 33, e4862.

Abdollahi-Alibeik M., Gharibpour N., Ramazani Z., Magnetically recoverable nanostructured Pd complex of dendrimeric type ligand on the MCM-41: Preparation, characterization and catalytic activity in the Heck reaction. Main Group Met. Chem., 2020, 43, 184–199.

Abdollahi-Alibeik M., Moaddeli A., Multi-component one-pot reaction of aldehyde, hydroxylamine and sodium azide catalyzed by Cu-MCM-41 nanoparticles: A novel method for the synthesis of 5-substituted 1H-tetrazole derivatives. New J. Chem., 2015, 39, 2116–2122.

Abdollahi-Alibeik M., Rezaeipoor-Anari A., Fe_3O_4@B-MCM-41: A new magnetically recoverable nanostructured catalyst for the synthesis of polyhydroquinolines. J. Magn. Magn. Mater., 2016, 398, 205–214.

Adlnasab L., Ezoddin M., Karimi M.A., Hatamikia N., MCM-41@Cu–Fe–LDH magnetic nanoparticles modified with cationic surfactant for removal of Alizarin Yellow from water samples and its determination with HPLC. Res. Chem. Intermed., 2018, 44, 3249–3265.

Bahrami S., Hassanzadeh-Afruzi F., Maleki A., Synthesis and characterization of a novel and green rod-like magnetic ZnS/$CuFe_2O_4$/agar organometallic hybrid catalyst for the synthesis of biologically-active 2-amino-tetrahydro-4H-chromene-3-carbonitrile derivatives. Appl. Organomet. Chem., 2020, 34. e5949.

Cha J.H., Choi H.-H., Jung Y.-G., Choi S.-C., An G.S., Novel synthesis of core–shell structured Fe_3O_4@ SiO_2 nanoparticles via sodium silicate. Ceram. Int., 2020, 46(10), 14384–14390.

Chatterjee S., Li X.S., Liang F., Yang Y.W., Design of multifunctional fluorescent hybrid materials based on SiO_2 materials and core–shell Fe_3O_4@SiO_2 nanoparticles for metal ion sensing. Small, 2019, 15, 1904569.

Chen J., Dai L., Li J., Mohammadnia M., Pd based on 2-Aminopyrimidine and 1H-benzo [d] imidazol-2-amine functionalized Fe_3O_4 nanoparticles as novel recyclable magnetic nanocatalysts for Ullmann coupling reaction. Appl. Organomet. Chem., 2020, 34, e5708.

Chen L., Gao Z., Li Y., Immobilization of Pd (II) on MOFs as a highly active heterogeneous catalyst for Suzuki–Miyaura and Ullmann-type coupling reactions. Catal. Today, 2015, 245, 122–128.

Chen Y., Mu S., Core–shell structured Fe_3O_4 nanoparticles functionalized with rhodamine derived probe for the detection, adsorption and removal of Hg (II): a sensing system with 'warning'signal. Sens. Actuators, B, 2014, 192, 275–282.

Dai J., Zhao W., Xing L., Shang J., Ju H., Zhou X., Zhu J., Dechlorinated Ullmann coupling reaction of aryl chlorides on Ag (111): A combined STM and XPS study. ChemPhysChem., 2019, 20, 2367–2375.

Daneshafruz H., Barani H., Sheibani H., Palladium nanoparticles-decorated β-cyclodextrin–cyanoguanidine modified graphene oxide: A heterogeneous nanocatalyst for suzuki–miyaura coupling and reduction of 4-nitrophenol reactions in aqueous media. J. Inorg. Organomet. Polym. Mater., 2022, 32, 791–802.

Eivazzadeh-Keihan R., Aliabadi H.A., Radinekiyan F., Sobhani M., Maleki A., Madanchi H., et al., Investigation of the biological activity, mechanical properties and wound healing application of a novel scaffold based on lignin–agarose hydrogel and silk fibroin embedded zinc chromite nanoparticles. RSC Adv., 2021, 11, 17914–17923.

Elhamifar D., Ramazani Z., Norouzi M., Mirbagheri R., Magnetic iron oxide/phenylsulfonic acid: a novel, efficient and recoverable nanocatalyst for green synthesis of tetrahydrobenzo [b] pyrans under ultrasonic conditions. J. Colloid Interface Sci., 2018, 511, 392–401.

Esrafili L., Morsali A., Dehghani Firuzabadi F., Retailleau P., Development of porous cobalt-/copper-doped carbon nanohybrids derived from functionalized mofs as efficient catalysts for the Ullmann cross-coupling reaction: insights into the active centers. ACS Appl. Mater. Interfaces, 2020, 12, 43115–43124.

Galeotti G., Di Giovannantonio M., Cupo A., Xing S., Lipton-Duffin J., Ebrahimi M., et al., An unexpected organometallic intermediate in surface-confined Ullmann coupling. Nanoscale, 2019, 11, 7682–7689.

Hajian R., Ehsanikhah A., Manganese porphyrin immobilized on magnetic MCM-41 nanoparticles as an efficient and reusable catalyst for alkene oxidations with sodium periodate. Chem. Phys. Lett., 2018, 691, 146–154.

Hashemi-Uderji S., Abdollahi-Alibeik M., Ranjbar-Karimi R., Fe_3O_4@FSM-16-SO_3H as a new magnetically recyclable nanostructured catalyst: Synthesis, characterization and catalytic application for the synthesis of pyrano [2,3-c]pyrazoles. Iranian J. Catal., 2018a, 8, 311–323.

Hashemi-Uderji S., Abdollahi-Alibeik M., Ranjbar-Karimi R., Fe_3O_4@FSM-16-SO_3H as a novel magnetically recoverable nanostructured catalyst: preparation, characterization and catalytic application. J. Porous Mater., 2018b, 26, 467–480.

Hashemi-Uderji S., Abdollahi-Alibeik M., Ranjbar-Karimi R., FSM-16-SO_3H nanoparticles as a novel heterogeneous catalyst: Preparation, characterization, and catalytic application in the synthesis of polyhydroquinolines. Main Group Met. Chem., 2018c, 41, 91–101.

Hemmati S., Ahany Kamangar S., Yousefi M., Hashemi Salehi M., Hekmati M., Cu (I)-anchored polyvinyl alcohol coated-magnetic nanoparticles as heterogeneous nanocatalyst in Ullmann-type C–N coupling reactions. Appl. Organomet. Chem., 2020, 34, e5611.

Hosseinian A., Nezhad P.D.K., Ahmadi S., Rahmani Z., Monfared A., A walk around the decarboxylative CS cross-coupling reactions. J. Sulfur Chem., 2019, 40, 88–112.

Javid A., Moeinpour F., Ni0. 5Zn0. 5Fe_2O_4@ HA-PRS nanoparticle: A recoverable green catalyst for the synthesis of tetrahydrobenzo [b] pyrans in water. Bull. Chem. Soc. Ethiop., 2018, 32, 501–511.

Karimi B., Barzegar H., Vali H., Au-Pd bimetallic nanoparticles supported on a high nitrogen-rich ordered mesoporous carbon as an efficient catalyst for room temperature Ullmann coupling of aryl chlorides in aqueous media. Chem. Commun. (Camb.)., 2018, 54, 7155–7158.

Khalili D., Rezaei M., Koohgard M., Ligand-free copper-catalyzed O-arylation of aryl halides using impregnated copper ferrite on mesoporous graphitic carbon nitride as a robust and magnetic heterogeneous catalyst. Microporous Mesoporous Mater., 2019, 287, 254–263.

Khalilzadeh M.A., Tajik S., Beitollahi H., Venditti R.A., Green synthesis of magnetic nanocomposite with iron oxide deposited on cellulose nanocrystals with copper (Fe_3O_4@CNC/Cu): investigation of catalytic activity for the development of a venlafaxine electrochemical sensor. Ind. Eng. Chem. Res., 2020, 59, 4219–4228.

Khodaei M.M., Alizadeh A., Haghipour M., Preparation and characterization of isatin complexed with Cu supported on 4-(aminomethyl) benzoic acid-functionalized Fe_3O_4 nanoparticles as a novel magnetic catalyst for the Ullmann coupling reaction. Res. Chem. Intermed., 2019, 45, 2727–2747.

Kitanovski A., Energy Applications of Magnetocaloric Materials. Adv. Energy Mate., 2020, 10, 1903741.

Liu X., Mi W., Zhang Q., Zhang X., Negative differential resistance and magnetotransport in Fe_3O_4/SiO_2/Si heterostructures. Appl. Phys. Lett., 2019, 114, 242402.

Maleki A., Fe_3O_4/SiO_2 nanoparticles: an efficient and magnetically recoverable nanocatalyst for the one-pot multicomponent synthesis of diazepines. Tetrahedron, 2012, 68, 7827–7833.

Maleki A., One-pot multicomponent synthesis of diazepine derivatives using terminal alkynes in the presence of silica-supported superparamagnetic iron oxide nanoparticles. Tetrahedron Lett., 2013, 54, 2055–2059.

Maleki A., One-pot three-component synthesis of pyrido[2′,1′:2,3] imidazo[4,5-c]isoquinolines using $Fe_3O_4@SiO_2$–OSO_3H as an efficient heterogeneous nanocatalyst. RSC Adv., 2014, 4, 64169–64173.

Maleki A., Green oxidation protocol: Selective conversions of alcohols and alkenes to aldehydes, ketones and epoxides by using a new multiwall carbon nanotube-based hybrid nanocatalyst via ultrasound irradiation. Ultrason. Sonochem., 2018, 40, 460–464.

Maleki A., Azadegan S., Amine-functionalized silica-supported magnetic nanoparticles: Preparation, characterization and catalytic performance in the chromene synthesis. J. Inorg. Organomet. Polym. Mater., 2017, 27, 714–719.

Maleki A., Panahzadeh M., Eivazzadeh-keihan R., Agar: a natural and environmentally-friendly support composed of copper oxide nanoparticles for the green synthesis of 1,2,3–triazoles. Green Chem. Lett. Rev., 2019, 12, 395–406.

Maleki A., Taheri-Ledari R., Ghalavand R., Design and fabrication of a magnetite-based polymer-supported hybrid nanocomposite: a promising heterogeneous catalytic system utilized in known palladium-assisted coupling reactions. Comb. Chem. High Throughput Screening, 2020, 23, 119–125.

Maleki A., Taheri-Ledari R., Ghalavand R., Firouzi-Haji R., Palladium-decorated o-phenylenediamine-functionalized Fe_3O_4/SiO_2 magnetic nanoparticles: A promising solid-state catalytic system used for Suzuki–Miyaura coupling reactions. J. Phys. Chem. Solids, 2020, 136, 109200–109201.

Maleki B., Alinezhad H., Atharifar H., Tayebee R., Mofrad A.V., One-Pot Synthesis of Polyhydroquinolines Catalyzed by $ZnCl_2$ Supported on Nano Fe_3O_4/SiO_2. Org. Prep. Proced. Int., 2019, 51, 301–309.

Moaddeli A., Abdollahi-Alibeik M., A nano magnetically mesoporous catalyst for the synthesis of propargylamine derivatives. J. Porous Mater., 2017, 25, 1–13.

Nasrallah G.K., Zhang Y., Zagho M.M., Ismail H.M., Al-Khalaf A.A., Prieto R.M., et al., A systematic investigation of the bio-toxicity of core-shell magnetic mesoporous silica microspheres using zebrafish model. Microporous Mesoporous Mater., 2018, 265, 195–201.

Niemelä K., Identification of novel cellulose degradation products. Acta Chem. Scand. B, 1987, 41, 257–260.

Nikoorazm M., Erfani Z., Core–shell nanostructure (Fe_3O_4@MCM-41@Cu-P2C) as a highly efficient and recoverable nanocatalyst for the synthesis of polyhydroquinoline, 5-substituted 1H-tetrazoles and sulfides. Chem. Phys. Lett., 2019, 737, 136784.

Nikoorazm M., Ghorbani F., Ghorbani-Choghamarani A., Erfani Z., Nickel Schiff base complex anchored on Fe3O4@MCM-41 as a novel and reusable magnetic nanocatalyst and its application in the oxidation of sulfides and oxidative coupling of thiols using H_2O_2. Phosphorus, Sulfur Silicon Relat. Elem., 2018, 193, 552–561.

Nikoorazm M., Ghorbani F., Ghorbani-Choghamarani A., Erfani Z., Pd (0)-S-propyl-2-aminobenzothioate immobilized onto functionalized magnetic nanoporous MCM-41 as efficient and recyclable nanocatalyst for the Suzuki, Stille and Heck cross coupling reactions. Appl. Organomet. Chem., 2018, 32, e4282.

Norouzi M., Elhamifar D., Mirbagheri R., Ramazani Z., Synthesis, characterization and catalytic application of a novel ethyl and boron sulfonic acid based bifunctional periodic mesoporous organosilica. J. Taiwan Inst. Chem. Eng., 2018, 89, 234–244.

Ohtaka A., Sakon A., Yasui A., Kawaguchi T., Hamasaka G., Uozumi Y., Nomura R., Catalytic specificity of linear polystyrene-stabilized Pd nanoparticles during Ullmann coupling reaction in water and the associated mechanism. J. Organomet. Chem., 2018, 854, 87–93.

Ojaghi Aghbash K., Noroozi Pesyan N., Batmani H., Fe_3O_4@silica-MCM-41@DABCO: A novel magnetically reusable nanostructured catalyst for clean in situ synthesis of substituted 2-aminodihydropyrano [3, 2-b] pyran-3-cyano. Appl. Organomet. Chem. 2019, 33, e5227.

Pourhasan-Kisomi R., Shirini F., Golshekan M., Organic/inorganic Fe_3O_4@MCM-41@Zr-piperazine: an impressive magnetite nanocatalyst for N-tert-butoxycarbonylation of amines. J. Nanosci. Nanotechnol., 2019, 19, 3859–3870.

Ramazani Z., Elhamifar D., Norouzi M., Mirbagheri R., Magnetic mesoporous MCM-41 supported boric acid: A novel, efficient and ecofriendly nanocomposite. Composites Part B, 2019, 164, 10–17.

Reiss P., Protiere M., Li L., Core/shell semiconductor nanocrystals. Small, 2009, 5, 154–168.

Rodríguez-Fernández J., Schmidt S.B., Lauritsen J.V., Sulfur-driven switching of the Ullmann coupling on Au (111). Chem. Commun., 2018, 54, 3621–3624.

Sakata K., Wang Y., Urabe D., Inoue M., Synthesis of the tetracyclic structure of batrachotoxin enabled by bridgehead radical coupling and Pd/Ni-promoted Ullmann reaction. Org. Lett., 2018, 20, 130–133.

Seyedi N., Shahabi Nejad M., Saidi K., Sheibani H., Fabrication of nitrogen-enriched graphene oxide/Cu NPs as a highly efficient and recyclable heterogeneous nanocatalyst for the Chan–Lam cross-coupling reaction. Appl. Organomet. Chem., 2019, 34. e5307.

Seyednejhad S., Khalilzadeh M.A., Zareyee D., Sadeghifar H., Venditti R., Cellulose nanocrystal supported palladium as a novel recyclable catalyst for Ullmann coupling reactions. Cellulose, 2019, 26, 5015–5031.

Sobhan Ardakani S., Cheraghi M., Jafari A., Zandipak R., PECVD synthesis of ZnO/Si thin film as a novel adsorbent for removal of azithromycin from water samples. Int. J. Environ. Anal. Chem., 2020, 1–18.

Stöber W., Fink A., Bohn E., Controlled growth of monodisperse silica spheres in the micron size range. J. Colloid Interface Sci., 1968, 26, 62–69.

Ulu A., Noma S.A.A., Koytepe S., Ates B., Magnetic Fe3O4@ MCM-41 core–shell nanoparticles functionalized with thiol silane for efficient l-asparaginase immobilization. Artif. Cells Nanomed. Biotechnol., 2018, 46, 1035–1045.

Vahidian M., Elhamifar D., Shaker M., Core–shell structured magnetic mesoporous silica-titania: A novel, powerful and recoverable nanocatalyst. Polyhedron, 2020, 178, 114326.

Wang G., Wu Z., Liang Y., Liu W., Zhan H., Song M., , et al., Exploring the coordination confinement effect of divalent palladium/zero palladium doped polyaniline-networking: As an excellent-performance nanocomposite catalyst for CC coupling reactions. J. Catal., 2020, 384, 177–188.

Wang P., Kong A., Wang W., Zhu H., Shan Y., Facile preparation of ionic liquid functionalized magnetic nano-solid acid catalysts for acetalization reaction. Catal. Lett., 2010, 135, 159–164.

Wang W., Chen S., Cal E.G., Moro M.M., Moya S., Coy E., et al., ZIF-8-based vs. ZIF-8-derived Au and Pd nanoparticles as efficient catalysts for the Ullmann homocoupling reaction. Inorg. Chem. Front., 2020, 7, 3945–3952.

Xie W., Han Y., Wang H., Magnetic Fe_3O_4/MCM-41 composite-supported sodium silicate as heterogeneous catalysts for biodiesel production. Renew. Energ., 2018, 125, 675–681.

Yavari I., Mobaraki A., Hosseinzadeh Z., Sakhaee N., Copper-catalyzed Mizoroki-Heck coupling reaction using an efficient and magnetically reusable Fe_3O_4@SiO_2@ PrNCu catalyst. J. Organomet. Chem., 2019, 897, 236–246.

Zarei M., Seyedi N., Maghsoudi S., Shahabi Nejad M., Sheibani H., Synthesis of star-shaped CuO nanoparticles supported on magnetic functionalized graphene: Catalytic and antibacterial activity. J. Chinese Chem. Soc., 2020, 67, 1992–2003.

Zhang F., Wu X., Liang C., Li X., Wang Z., Li H., Highly active, water-compatible and easily separable magnetic mesoporous Lewis acid catalyst for the Mukaiyama–Aldol reaction in water. Green Chem., 2014, 16, 3768–3777.